Soft Matter

PAPER

View Article Online
View Journal | View Issue

Cite this: *Soft Matter*, 2023, **19**, 4519

Effect of poly[oligo(ethylene glycol) methyl ether methacrylate] side chain length on the brush swelling behavior in A/B/A–B ternary blends with polystyrene†

Caini Zheng,[a] Bo Zhang,[b] Frank S. Bates*[b] and Timothy P. Lodge*[ab]

Received 7th February 2023,
Accepted 28th May 2023

DOI: 10.1039/d3sm00151b

rsc.li/soft-matter-journal

The phase behavior of ternary blends composed of two homopolymers (A, B) and their corresponding diblock copolymer (A–B) has been widely studied, with emphasis on the volumetrically symmetric isopleth and the formation of bicontinuous microemulsions. However, almost all the previous studies employed linear polymers, and little is known about the impact of polymer architecture on the phase behavior of such ternary blends. Here, we report the self-assembly of three sets of ternary blends of polystyrene (PS) and poly[oligo(ethylene glycol) methyl ether methacrylate] (POEGMA$_n$), with different lengths of oligo(ethylene glycol) side chains n. Small-angle X-ray scattering was used to probe the phase behavior at different compositions and temperatures. The order-to-disorder transition temperature was found to be impacted by the side chain length. It was also observed that longer side chains lead to poorer miscibility of homopolymers in the corresponding block, resulting in a more "dry-brush" like swelling behavior.

Introduction

Traditional liquid electrolytes in lithium-ion batteries pose great safety concerns due to their flammability and potential dendrite growth.[1] Recently, polymer-based electrolytes have attracted major interest and are candidates for next-generation battery electrolytes.[2,3] A critical challenge is to promote ionic conductivity and mechanical integrity simultaneously, where the former typically demands flexible segmental motion and the latter requires solid polymers. One solution is to prepare nanostructured polymeric materials featuring two interpenetrating domains with different chemical structures. Despite the abundant phase diagrams of pure block copolymers, preparation of three-dimensional co-continuous phases, such as the double gyroid, poses synthetic challenges due to their narrow composition windows.[4–9] Alternatively, ready access to co-continuous network phases can be achieved by blending block copolymers (A–B) and homopolymers (A, B) with simple variation of volumetric ratios.[10–12] In addition to traditional network phases in block copolymers, the polymeric bicontinuous microemulsions (BμE), analogous to co-continuous microemulsions in water/oil/surfactant systems with locally correlated interfaces but global disorder, have also been widely reported in A/B/A–B ternary blends.[13–20] BμE features a typical phase window of $\Delta\phi_H \sim$ 1–5% ($\phi_H = \phi_A + \phi_B$), where ϕ_i denotes the volume fraction of component i. Furthermore, typical domain sizes in the BμE are 50–200 nm, significantly larger than can be conveniently accessed in typical double gyroid materials. Since its discovery in 1997,[13] the BμE has been studied in polymeric ternary blends with focuses on the effects of polymer chemistry,[15] polymer composition,[21–23] dispersity,[24,25] conformational asymmetry,[26] and charge.[27–29] However, little is yet known about how polymer architecture affects the formation of BμE.

For applications as polymer electrolytes, poly(ethylene oxide) (PEO), which is well recognized to possess superior ion-conducting properties with added salt, has been studied as the conducting domain in the BμE, with polystyrene (PS) as the neutral component.[27–29] In a recent study by Xie *et al.*, lithium bis-(trifluoromethane) sulfonimide doped ternary blends (PEO/PS/PEO–PS) were prepared and conductivity was examined upon increasing the homopolymer content.[28] The BμE was found to exhibit higher conductivity compared with LAM and nonstructured disordered blends, which is attributed to the continuous conducting domains and elimination of fixed domain boundaries. However, the room-temperature performance of PEO is undermined by relatively slow segmental

[a] *Department of Chemistry, University of Minnesota, Minneapolis, MN 55455, USA. E-mail: lodge@umn.edu*
[b] *Department of Chemical Engineering and Materials Science, University of Minnesota, Minneapolis, MN 55455, USA. E-mail: bates001@umn.edu*

† Electronic supplementary information (ESI) available. See DOI: https://doi.org/10.1039/d3sm00151b

motion and by crystallinity. One possible solution is to install low-molecular-weight PEO as side chains attached to a backbone, in comb- or brush-like structures, where the crystallinity of the PEO domain is largely suppressed especially with short PEO side chains.[30–35] In such PEO-grafted systems, ion transport is found to occur through inter- and intra-side chain hopping according to a recent study by Deng *et al.*[36] However, most attention has focused on the crystallization behavior and conductivity performance of PEO-branched homopolymers or block polymers; our emphasis is on the effect of the side chain architecture on polymer–polymer interactions and packing, which are essential to the rational design of the BμE in ternary blends.

The miscibility of homopolymers in block polymer/homopolymer blends is known to greatly impact phase behavior. A series of works by Hashimoto and coworkers investigated the swelling behavior upon adding homopolymers in binary (A + A–B) and ternary (A + B + A–B) blends.[37–40] Depending on the relative length of homopolymers added, two swelling limits, ''wet-brush'' ($\alpha \ll 1$) or ''dry-brush'' ($\alpha \gtrsim 1$) scenarios were discussed, where α is the ratio of the volumetric degree of polymerization (N) between the homopolymer and block polymer ($\alpha = N_h/N_{bp}$). In the ''wet-brush'' case, homopolymers distribute uniformly in the corresponding block, while in the ''dry-brush'' limit they are excluded from the block copolymer brushes. The difference in the homopolymer solubility results in different interfacial curvature and variation in domain size. In practice, many systems lie between these two extremes, where equilibrium states exist with homopolymers distributed partially inside and outside the block copolymer brushes. Multiple experimental and theoretical works reported that increasing α ($\alpha \lesssim 1$) results in a rapid growth in the domain size, as a result of more homopolymers localizing in the interdomain due to an increase in the conformational entropic penalty.[41–45] In linear polymers, increasing N_h has been proven to be effective in driving the swelling behavior from wet-brush behavior toward the dry-brush limit. On the other hand, polymer architecture is expected to have a significant impact on the mixing of homopolymers and diblock copolymers, given the conformational entropy change upon swelling.

In this paper, three families of ternary blends composed of poly[oligo(ethylene glycol) methyl ether methacrylate] (POEGMA$_n$)/polystyrene (PS)/POEGMA$_n$–PS were prepared, where n denotes the average number of EO repeat units per POEGMA side chain. The resulting phase behavior was examined using small-angle X-ray scattering (SAXS) along the volumetrically symmetric isopleth, where the two homopolymer volume fractions are equal. Macrophase separation was found to extend to regions with lower homopolymer content with longer side chains. Furthermore, a direct comparison of the relative domain size change reveals a more ''dry-brush'' like swelling behavior in ternary systems with longer side chains.

Experimental

POEGMA$_n$–PS block polymers and POEGMA$_n$ homopolymers were synthesized using reversible-addition-fragmentation chain-transfer (RAFT) polymerization, followed by removal of the reactive end group.[48] Polystyrene homopolymers were purchased and used as received (Sigma-Aldrich). Chemical structures of the polymers were confirmed by proton nuclear magnetic resonance spectroscopy (^{1}H NMR), while molecular weights (M_n) and dispersities ($Đ$) were determined through size exclusion chromatography (SEC) equipped with multi-angle light scattering (MALS). Detailed polymer characterization is summarized in Table 1. After blending, polymer samples were sealed in Tzero pans filled with argon and annealed before SAXS experiments were conducted at different temperatures. For the determination of macrophase separation, polymer samples were sealed in transparent ampules and heated to the target temperature, where the turbidity of the sample is examined visually. Synthesis and characterization details can be found in the ESI.†

Results and discussion

Three sets of polymer blends composed of POEGMA$_n$–PS/POEGMA$_n$/PS were prepared, and will be referred to as T1, T2, and T3 (see Table 1). The average # of EO side chain repeat units on the POEGMA block n = 1, 4.5, and 9.1, respectively. The phase behavior was studied by SAXS at various temperatures ranging

Table 1 Polymer characteristics

Blend	Name	M_n[a] (kDa)	f_{POEGMA}[b]	$Đ$[a] = M_w/M_n	ρ (g cm^{-3})	N[c]	α[d]	# of EO repeating units
T1	POEGMA$_1$–PS	25	0.49	1.03	1.08[f]	380		1
	POEGMA$_1$	5.2		1.06	1.11[g]	77	0.20	
	PS-5k	5.1		1.04	1.05[h]	80	0.21	
T2	POEGMA$_{4.5}$–PS	28	0.53	1.11	1.07[f]	436		4.5
	POEGMA$_{4.5}$	6.8		1.08	1.08[g]	104	0.24	
	PS-6k	6.4		1.05[e]	1.05	101	0.23	
T3	POEGMA$_{9.1}$–PS	27	0.52	1.09	1.06[f]	418		9.1
	POEGMA$_{9.1}$	6.9		1.08	1.06[g]	108	0.26	
	PS-6k	6.3		1.01	1.05	100	0.24	

[a] Determined from SEC-MALS. [b] Volume fraction of POEGMA block determined by ^{1}H NMR spectroscopy. [c] Degree of polymerization calculated based on a reference volume of 0.1 nm^3. [d] $\alpha = N_h/N_{bp}$. [e] From supplier. [f] Calculated by assuming the density of each block equals that of the homopolymer. [g] Estimated based on group contribution method.[46] [h] Obtained from the reference.[47]

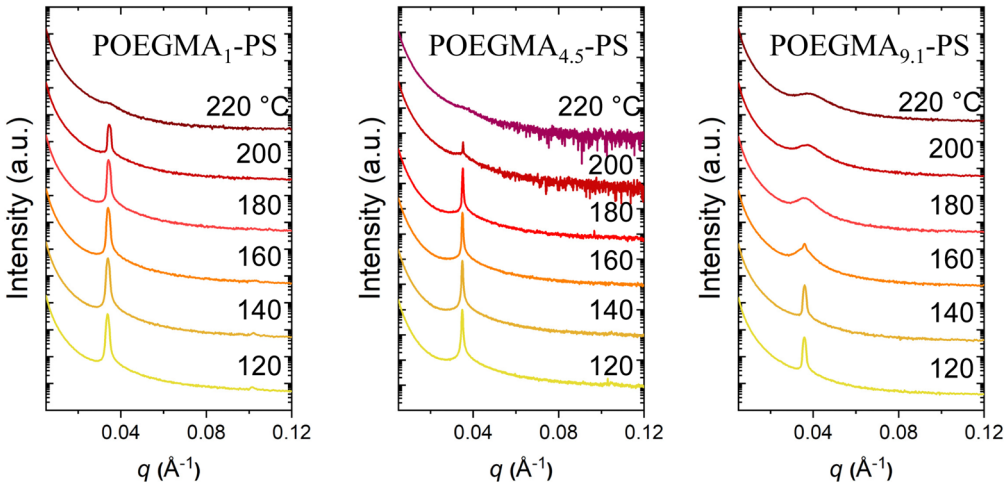

Fig. 1 Scattering profiles for block copolymers POEGMA$_1$–PS, POEGMA$_{4.5}$–PS and POEGMA$_{9.1}$–PS at different temperatures.

from 120–220 °C, at intervals of 20 °C. As shown in Fig. 1, POEGMA$_1$–PS and POEGMA$_{4.5}$–PS exhibit a lamellar (LAM) phase as indicated by $q/q^* = 1, 2, 3\ldots$, where q is the scattering wavevector and q^* is the primary peak position. It should be noted that the second peak is absent in both scattering profiles due to structure factor extinction from the nearly symmetric copolymers.[49] No higher order peaks were observed in POEGMA$_{9.1}$–PS, but a LAM phase is assumed given the symmetric composition of the block copolymer. Order-to-disorder transitions (ODT) were observed for all three block copolymers, where the sharp primary peak of the LAM phase turns into a broad peak, indicating a disordered (DIS) phase. POEGMA$_1$–PS, which has a smaller total M_n, exhibits a comparable or higher order-to-disorder transition temperature (T_{ODT}) (200–220 °C) than POEGMA$_{4.5}$–PS (200–220 °C) and POEGMA$_{9.1}$–PS (~160 °C). Such behavior indicates a stronger segregation strength between PS and POEGMA$_n$ when the side chain is shorter. This is opposite to the prediction from the Flory–Huggins parameters (χ) between PS/poly(methyl methacrylate) (PMMA) and PS/PEO, if one considers POEGMA to be a PEO/PMMA copolymer. Based on a reference volume of 118 Å^3, $\chi_{PS-PMMA} = 3.5\ (K)/T + 0.022$ while $\chi_{PS-PEO} = 29.8\ (K)/T - 0.023$ as reported by previous studies.[50–53] For the temperature range studied here, $\chi_{PS-PMMA}$ is predicted to be smaller than χ_{PS-PEO}, indicating a stronger incompatibility between styrene and EO monomers. This discrepancy implies that the effective χ is reduced by the side chains, where longer side chains lead to fewer contacts between styrene and EO units nearer to the backbone. The reduced contacts between incompatible units lowers the enthalpic penalty of mixing, with a concomitant reduction in χ. With the side chain increasing from 4.5 to 9.1 EO repeating units, direct comparison is unavailable due to the change in both M_n and T_{ODT}. However, little change in χ is expected as EO repeating units in both polymers are largely shielded from the PS/POEGMA interface.

Upon blending equal volumes of A and B homopolymers with a symmetric A–B block copolymer, the homopolymers reside in the corresponding domain and swell the LAM structure. As a result, the domain size increases, which is reflected by the decrease in q^* in Fig. 2. At a higher homopolymer volume fraction ϕ_H ($\phi_H = \phi_{POEGMA_n} + \phi_{PS}$), a transition from LAM to DIS is observed in T3 when ϕ_H increases from 0.70 to 0.75, which is attributable to the formation of a BμE phase. To further investigate the phase behavior of these ternary blends, three volumetrically symmetric isopleths were constructed, as shown in Fig. 3. As ϕ_H increases, T_{ODT} decreases in the case of T1, while it increases in T2 and T3. It should be noted that the α value (Table 1) for T2 and T3 is close to 0.25 whereas α is about 0.20 for T1. Shorter homopolymers are considered to destabilize the ordered structure with greater entropic gain upon the transition from order to disorder, whereas blending larger homopolymers raises the incompatibility of the system. Such a transition from decreasing to increasing T_{ODT} with respect to homopolymer length is predicted to take place around $\alpha = 0.25$.[54] On the other hand, as the critical temperature of a homopolymer blend, (*i.e.*, the temperature above which the homopolymers become completely miscible), increases with molecular weight, blending a block copolymer with longer homopolymers is also expected to enhance the T_{ODT}.

The emergence of the BμE is widely reported near the mean-field-theory-predicted Lifshitz point ($\phi_H = 1/(1 + 2\alpha^2)$) in symmetric linear ternary blends.[54] In T1 and T2, a pure BμE phase is not observed, which can be a result of either a narrow phase window, or being pre-empted by macrophase separation. In T1, a turbid sample is obtained at $\phi_H = 0.83$, implying a BμE phase window $\Delta\phi_H < 3\%$. In T3, broad peaks are observed in the scattering profiles at $\phi_H = 0.7$ above 120 °C as shown in Fig. 4. The structure of the BμE at various temperatures was further examined by fitting the scattering data with Teubner–Strey model (eqn (1)), where I is the scattering intensity and a_2, c_1 and c_2 are the fitting parameters.[55] A negative c_1 indicates a tendency toward forming interfaces and is characteristic of a BμE phase. The amphiphilicity factor (f_a), which reflects the BμE structure, can also be extracted based on eqn (2).

$$I(q) = \frac{1}{a_2 + c_1 q^2 + c_2 q^4} \quad (1)$$

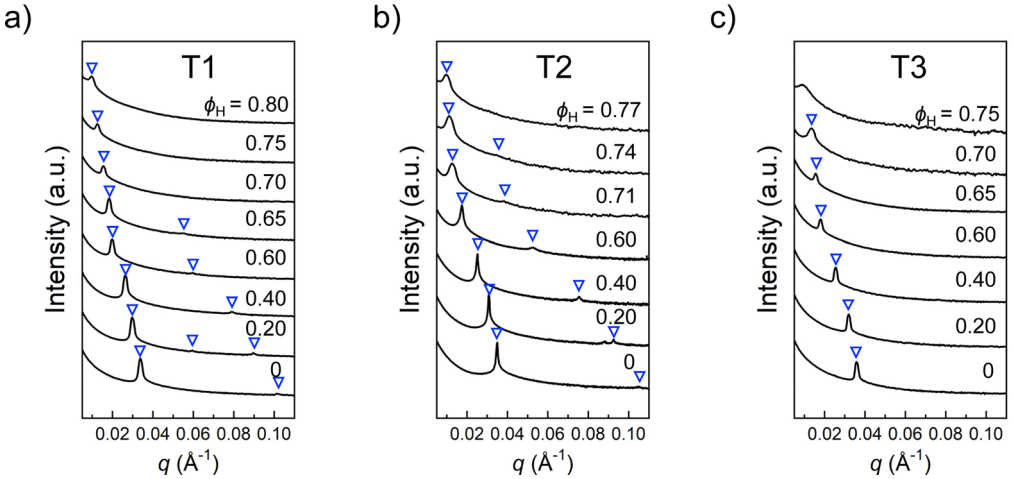

Fig. 2 SAXS patterns for ternary blends (a) T1, (b) T2, and (c) T3 along the isopleth at various ϕ_H at 120 °C. The triangles indicate the peaks assigned for LAM phase.

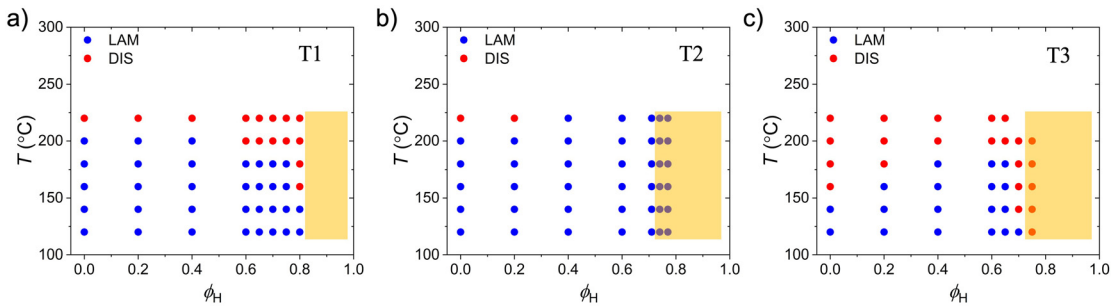

Fig. 3 Volumetrically symmetric isopleth for (a) T1, (b) T2, and (c) T3 based on SAXS results. Macrophase separation is represented by shaded areas (yellow) and was determined based on visual observation.

$$f_a = \frac{c_1}{\sqrt{4a_2c_2}} \quad (2)$$

Specifically, f_a = −1 corresponds to LAM structure and for a "good" BμE, $-1 < f_a < 0$. As temperature changes from 140 to 200 °C, f_a increases from −0.85 to −0.62, indicating a less ordered structure. On the basis of optical turbidity, another prominent feature is the large window of phase coexistence on the homopolymer-rich side for T2 and T3, which extends down to $\phi_H \sim 0.75$. Note that in linear polymer systems with similar α values ($\alpha \sim 0.2$), the phase window of macrophase separation usually appears around $\phi_H \geq 0.9$.[56] This observation, however, is in accordance with our previous work, where macrophase separation extends to $\phi_H \sim 0.6$–0.7 in ternary blends consisting of symmetric poly[(oligo(ethylene glycol) methyl ether methacrylate-*co*-oligo(ethylene glycol) propyl sodium sulfonate methacrylate)], PS and the corresponding block copolymer.[57]

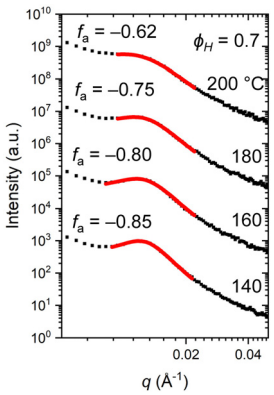

Fig. 4 SAXS profiles of T3 containing ϕ_H = 0.7 at various temperatures. The red lines represent the fitting of Teubner–Strey model (eqn (1)) and the amphiphilicity factor (f_a) is calculated based on eqn (2).

To further examine how differing side chain lengths affect the swelling behavior in this system, we plotted the relative domain size (d/d_0) change as a function of ϕ_H, where d is calculated based on eqn 3 and d_0 denotes the domain size of pure block copolymer. The result is shown in Fig. 5(a). Two swelling extremes, dry-brush (eqn (4)) and wet-brush (eqn (5)), are also plotted for comparison. For linear polymers in the wet-brush limit, where homopolymers are much smaller than the block copolymer ($\alpha \ll 1$), d grows slowly with the addition of homopolymers. This indicates that homopolymers penetrate the corresponding block and push the copolymer junctions

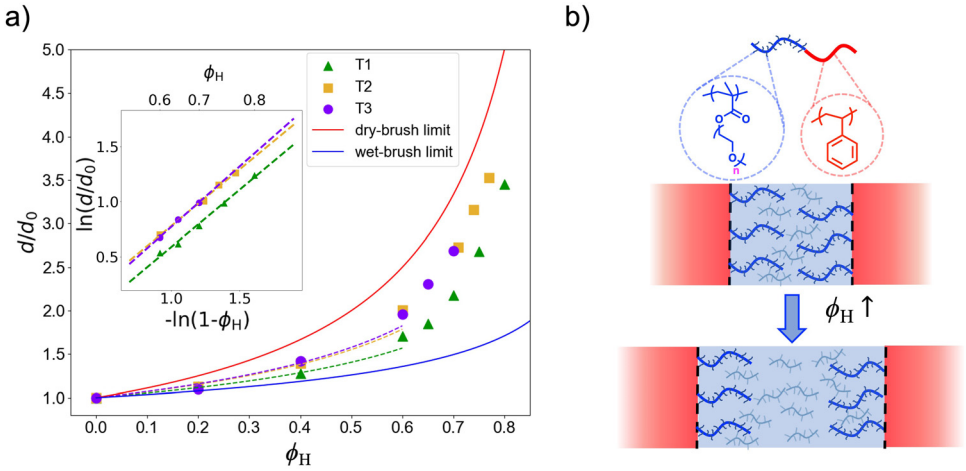

Fig. 5 (a) Relative domain size change along the volumetrically symmetric isopleth as a function of ϕ_H. Domain sizes are calculated for LAM samples. The blue line and red lines represent the wet and dry brush limits, respectively. The data are fit to $d/d_0 = (1-\phi_H)^{-A}$ with $\phi_H \leq 0.4$ (dashed lines) and $\ln(d/d_0) = -A\ln(1-\phi_H) + B$ at $\phi_H > 0.4$ (inserted figure), where A and B are fitting parameters. (b) Schematic representation of two-step swelling where the homopolymers are included and excluded from the block copolymer regime at low and high ϕ_H, respectively.

apart along the interface. On the other hand, in the dry-brush limit, homopolymers are excluded from the block copolymer and reside in the interdomain, which causes a more dramatic change in the domain size while the interfacial area remains unchanged.

$$d_{LAM} = \frac{2\pi}{q^*} \quad (3)$$

$$d/d_0 = (1-\phi_H)^{-1} \quad (4)$$

$$d/d_0 = (1-\phi_H)^{-1/3} \quad (5)$$

$$A_c = \frac{2M_{POEGMA_n\text{-}PS}}{N_A \rho_{POEGMA_n\text{-}PS}(1-\phi_H)d_{LAM}} \quad (6)$$

In this system, the relative domain size change obtained from the LAM phase lies between the two limits and suggests a two-step swelling process. As demonstrated in Fig. 5(a), the increase in d/d_0 is slower at lower ϕ_H for all three ternary blends, and then becomes more rapid as ϕ_H further increases. Quantitatively, data at low and high ϕ_H were fitted with $d/d_0 = (1-\phi_H)^{-A}$ and $\ln(d/d_0) = -A\log(1-\phi_H) + B$, respectively. In the latter equation, B is added to account for the initial swelling process.

The resulting fitting parameters A and exponential of B are summarized in Table 2. At low ϕ_H ($\phi_H \leq 0.4$), the swelling behavior is closer to the wet-brush limit, indicating a mixing between homopolymers and block copolymers in the corresponding domains. However, even in the low ϕ_H region, the parameter A is larger than 1/3 in all cases, which implies that either some POEGMA homopolymers are expelled and move into the domain center, or that the swelling of the brush acts to extend the POEGMA backbone normal to the interface. At larger ϕ_H ($\phi_H > 0.4$), d/d_0 increases more rapidly with ϕ_H, and all three systems behave like a dry-brush with fitting parameter A being near 1 (Table 2). During this stage, block copolymers can no longer absorb more homopolymers and all further homopolymers are expelled to the LAM interdomains, forming a homopolymer-rich region as demonstrated in Fig. 5(b). From the volume change, $d/d_0 = a_0 v/a v_0 = a_0/a(1-\phi_H)^{-1}$ where a and v denote the interfacial area and total volume, respectively. For pure dry-brush swelling, $a_0/a = 1$, as all homopolymers stay in the inter-domain and no expansion of interfacial area would be observed. Due to the initial wet-brush swelling step in our system, a change in the interfacial area is expected and reflected in a non-zero value of fitting parameter B (Table 2). To further investigate the relationship between B and the interfacial area change, we calculated the area per copolymer junction (A_c) from eqn (6), assuming a single phase. The values of $A_c(\phi_H = 0)/A_c(\phi_H = 0.6)$ are summarized in Table 2, which represents a_0/a at the starting point of dry-brush swelling. As expected, the exponential of parameter B is close to $A_c(\phi_H = 0)/A_c(\phi_H = 0.6)$ in each blend, which further supports the assumption of a two-step swelling process. The crossover where the ternary blends transition from a wet- to dry-brush behavior can be taken as the saturation composition for the POEGMA$_n$ block, a transition that has been previously observed in linear ternary blends.[58] The saturation composition of block A is anticipated when the total volume occupied by block A and homopolymer A reaches the pervaded volume of block A.[59] Further addition of homopolymer A into block A demands

Table 2 Summary of fitting parameters in Fig. 5(a)

n	A at low ϕ_H	A at high ϕ_H	exp(B)	$A_c(\phi_H = 0)/A_c(\phi_H = 0.6)$
1	0.49	1.0	0.64	0.68
4.5	0.63	1.0	0.78	0.80
9.1	0.66	1.1	0.72	0.78

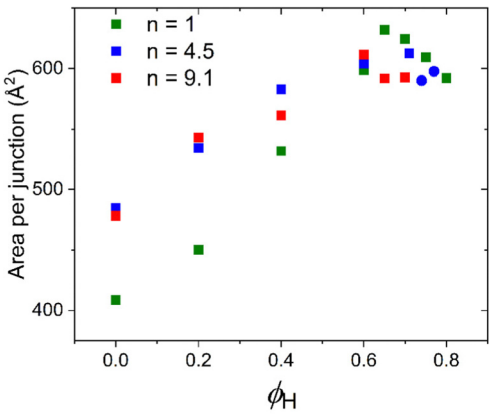

Fig. 6 Area per junction along the volumetrically symmetric isopleth for T1(green), T2 (blue), and T3 (red) as a function of ϕ_H. Change of symbols from square to circle represents the transition from optically clear to turbid blends.

chain stretching and is therefore entropically unfavored. A comparison among the three ternary blends reveals that in T1, the increase in d/d_0 in the initial swelling stage is more gradual than in T2 and T3, while the latter two share almost the same swelling profile. This is also reflected in a smaller A at low ϕ_H (0.49 compared with 0.63 and 0.66).

Given the similar α values for all three blends, we attribute the rapid growth of domain size in T2 and T3 to the presence of longer side chains on the POEGMA block. The POEGMA block becomes stiffer due to the crowding of side chains attached to the backbone. Swelling by homopolymer results in a greater loss of conformational entropy compared with linear systems. Moreover, when the side chain reaches 4.5 EO repeating units, the swelling behavior does not change much with longer side chains. It is likely that after reaching a certain point, the conformational entropy loss derived from the existence of the side chain saturates. We further plotted the change of A_c as a function of ϕ_H (see Fig. 6). The lateral dimension increases more rapidly for T1, indicating that homopolymers preferentially mix with the block copolymer and expand the spacing between junctions. On the other hand, T2 and T3 exhibit a much slower increase in the area per junction as more homopolymers are localized in the interdomain and contribute more to the perpendicular dimension growth, resulting in a dramatic change in d/d_0. At high ϕ_H, A_c becomes almost constant and fluctuates around a peak value. This coincides with the compositions where the systems approach the dry-brush limit, where homopolymers can no longer penetrate into the block copolymer and expand the lateral dimension.

Conclusion

In this study, we have investigated the phase behavior of three PS/POEGMA$_n$/PS–POEGMA$_n$ ternary blends with different side chain lengths on the POEGMA block. The brush-like POEGMA$_n$ block with longer side chains was found to stabilize the LAM structure, leading to an increased T_{ODT} along the isopleth. Analysis of the perpendicular and lateral dimensions with respect to the POEGMA/PS interface reveals that the longer side chains lead to poorer miscibility of homopolymers with the corresponding block. With a preference to reside in the interdomain, the increase in the perpendicular dimension is more dramatic in ternary blends with longer side chains. Overall, this work provides insights into the phase behavior and side-chain swelling behavior in A–B/A/B ternary systems with long side chains on one of the blocks. A possible direction of future research would be to blend grafted block copolymers with smaller homopolymers (*i.e.*, smaller α values) to locate the BμE phase, given the early appearance of macrophase separation in the current study.

Conflicts of interest

There are no conflicts to declare.

Acknowledgements

The work was supported by Award DE-SC0017809 funded by the U.S. Department of Energy (DOE), Office of Science. SAXS experiments were carried out in Sector 5 (DuPont-Northwestern-Dow Collaborative Access Team, DND-CAT) and Sector 12 of the Advanced Photon Source (APS). DND-CAT is supported by Northwestern University, The Dow Chemical Company, and DuPont de Nemours, Inc. This research used resources of the Advanced Photon Source, a U.S. DOE Office of Science User Facility operated for the DOE Office of Science by Argonne National Laboratory under contract no. DE-AC02-06CH11357. Parts of this work were carried out in the Characterization Facility, University of Minnesota, which receives partial support from the NSF through the MRSEC (award number DMR-2011401) and the NNCI (Award Number ECCS-2025124) programs.

References

1 J. Chen, *Materials*, 2013, **6**, 156–183.
2 H. Zhang, C. Li, M. Piszcz, E. Coya, T. Rojo, L. M. Rodriguez-Martinez, M. Armand and Z. Zhou, *Chem. Soc. Rev.*, 2017, **46**, 797–815.
3 S. N. Patel, *ACS Macro Lett.*, 2021, **10**, 141–153.
4 D. A. Hajduk, P. E. Harper, S. M. Gruner, C. C. Honeker, G. Kim, L. J. Fetters and G. Kim, *Macromolecules*, 1994, **27**, 4063–4075.
5 M. I. Kim, T. Wakada, S. Akasaka, S. Nishitsuji, K. Saijo, H. Hasegawa, K. Ito and M. Takenaka, *Macromolecules*, 2008, **41**, 7667–7670.
6 E. W. Cochran, C. J. Garcia-Cervera and G. H. Fredrickson, *Macromolecules*, 2006, **39**, 2449–2451.
7 L. Yan, C. Rank, S. Mecking and K. I. Winey, *J. Am. Chem. Soc.*, 2020, **142**, 857–866.
8 C. Zhai, H. Zhou, T. Gao, L. Zhao and S. Lin, *Macromolecules*, 2018, **51**, 4471–4483.

9 M. W. Matsen and M. Schick, *Phys. Rev. Lett.*, 1994, **72**, 2660–2663.
10 P. K. Janert and M. Schick, *Macromolecules*, 1997, **30**, 137–144.
11 N. R. Washburn, T. P. Lodge and F. S. Bates, *J. Phys. Chem. B*, 2000, **104**, 6987–6997.
12 R. J. Hickey, T. M. Gillard, M. T. Irwin, D. C. Morse, T. P. Lodge and F. S. Bates, *Macromolecules*, 2016, **49**, 7928–7944.
13 F. S. Bates, W. W. Maurer, P. M. Lipic, M. A. Hillmyer, K. Almdal, K. Mortensen, G. H. Fredrickson and T. P. Lodge, *Phys. Rev. Lett.*, 1997, **79**, 849–852.
14 G. H. Fredrickson and F. S. Bates, *J. Polym. Sci., Part B: Polym. Phys.*, 1997, **35**, 2775–2786.
15 M. A. Hillmyer, W. W. Maurer, T. P. Lodge, F. S. Bates and K. Almdal, *J. Phys. Chem. B*, 1999, **103**, 4814–4824.
16 D. Düchs, V. Ganesan, G. H. Fredrickson and F. Schmid, *Macromolecules*, 2003, **36**, 9237–9248.
17 B. Vorselaars, R. K. W. Spencer and M. W. Matsen, *Phys. Rev. Lett.*, 2020, **125**, 117801.
18 R. K. W. Spencer and M. W. Matsen, *Macromolecules*, 2021, **54**, 1329–1337.
19 N. Zhou, F. S. Bates and T. P. Lodge, *Nano Lett.*, 2006, **6**, 2354–2357.
20 B. H. Jones, K.-Y. Cheng, R. J. Holmes and T. P. Lodge, *Macromolecules*, 2012, **45**, 599–601.
21 G. Fleury and F. S. Bates, *Soft Matter*, 2010, **6**, 2751.
22 B. M. Habersberger, F. S. Bates and T. P. Lodge, *Soft Matter*, 2012, **8**, 3429–3441.
23 B. Zhang, S. Xie, T. P. Lodge and F. S. Bates, *Macromolecules*, 2021, **54**, 460–472.
24 R. B. Thompson and M. W. Matsen, *Phys. Rev. Lett.*, 2000, **85**, 670–673.
25 C. J. Ellison, A. J. Meuler, J. Qin, C. M. Evans, L. M. Wolf and F. S. Bates, *J. Phys. Chem. B*, 2009, **113**, 3726–3737.
26 N. Zhou, T. P. Lodge and F. S. Bates, *J. Phys. Chem. B*, 2006, **110**, 3979–3989.
27 M. T. Irwin, R. J. Hickey, S. Xie, S. So, F. S. Bates and T. P. Lodge, *Macromolecules*, 2016, **49**, 6928–6939.
28 S. Xie, D. J. Meyer, E. Wang, F. S. Bates and T. P. Lodge, *Macromolecules*, 2019, **52**, 9693–9702.
29 M. T. Irwin, R. J. Hickey, S. Xie, F. S. Bates and T. P. Lodge, *Macromolecules*, 2016, **49**, 4839–4849.
30 D. W. Xia and J. Smid, *J. Polym. Sci., Polym. Lett. Ed.*, 1984, **22**, 617–621.
31 J. M. G. Cowie, A. C. S. Martin and A.-M. Firth, *Br. Polym. J.*, 1988, **20**, 247–252.
32 A. Nishimoto, K. Agehara, N. Furuya, T. Watanabe and M. Watanabe, *Macromolecules*, 1999, **32**, 1541–1548.
33 A. J. Butzelaar, P. Röring, T. P. Mach, M. Hoffmann, F. Jeschull, M. Wilhelm, M. Winter, G. Brunklaus and P. Théato, *ACS Appl. Mater. Interfaces*, 2021, **13**, 39257–39270.
34 A. J. Butzelaar, K. L. Liu, P. Röring, G. Brunklaus, M. Winter and P. Theato, *ACS Appl. Polym. Mater.*, 2021, **3**, 1573–1582.
35 B. Kim, C.-G. Chae, Y. Satoh, T. Isono, M.-K. Ahn, C.-M. Min, J.-H. Hong, C. F. Ramirez, T. Satoh and J.-S. Lee, *Macromolecules*, 2018, **51**, 2293–2301.
36 C. Deng, M. A. Webb, P. Bennington, D. Sharon, P. F. Nealey, S. N. Patel and J. J. de Pablo, *Macromolecules*, 2021, **54**, 2266–2276.
37 H. Tanaka, H. Hascgawa and T. Hashimoto, *Macromolecules*, 1991, **24**, 240–251.
38 T. Hashimoto, H. Tanaka and H. Hasegawa, *Macromolecules*, 1990, **23**, 4378–4386.
39 H. Tanaka and T. Hashimoto, *Macromolecules*, 2002, **24**, 5713–5720.
40 S. Koizumi, H. Hasegawa and T. Hashimoto, *Makromol. Chem., Macromol. Symp.*, 1992, **62**, 75–91.
41 L. Messé, L. Corvazier and A. J. Ryan, *Polymer*, 2003, **44**, 7397–7403.
42 G. Liu, M. P. Stoykovich, S. Ji, K. O. Stuen, G. S. W. Craig and P. F. Nealey, *Macromolecules*, 2009, **42**, 3063–3072.
43 K. I. Winey, E. L. Thomas and L. J. Fetters, *Macromolecules*, 1991, **24**, 6182–6188.
44 M. W. Matsen, *Macromolecules*, 1995, **28**, 5765–5773.
45 K. Toth, S. Bae, C. O. Osuji, K. G. Yager and G. S. Doerk, *Macromolecules*, 2021, **54**, 7970–7986.
46 D. W. Van Krevelen and P. J. Hoftyzer, *J. Appl. Polym. Sci.*, 1969, **13**, 871–881.
47 J. E. Mark, *Physical properties of polymers handbook*, Springer, 2007, vol. 1076.
48 B. Zhang, C. Zheng, M. B. Sims, F. S. Bates and T. P. Lodge, *ACS Macro Lett.*, 2021, **10**, 1035–1040.
49 T. H. Epps, E. W. Cochran, T. S. Bailey, R. S. Waletzko, C. M. Hardy and F. S. Bates, *Macromolecules*, 2004, **37**, 8325–8341.
50 T. P. Russell, R. P. Hjelm and P. A. Seeger, *Macromolecules*, 1990, **23**, 890–893.
51 Y. Zhao, E. Sivaniah and T. Hashimoto, *Macromolecules*, 2008, **41**, 9948–9951.
52 J. G. Kennemur, M. A. Hillmyer and F. S. Bates, *Macromolecules*, 2012, **45**, 7228–7236.
53 E. W. Cochran, D. C. Morse and F. S. Bates, *Macromolecules*, 2003, **36**, 782–792.
54 D. Broseta and G. H. Fredrickson, *J. Chem. Phys.*, 1990, **93**, 2927–2938.
55 M. Teubner and R. Strey, *J. Chem. Phys.*, 1987, **87**, 3195–3200.
56 T. L. Morkved, B. R. Chapman, F. S. Bates, T. P. Lodge, P. Stepanek and K. Almdal, *Faraday Discuss.*, 1999, **112**, 335–350.
57 C. Zheng, B. Zhang, F. S. Bates and T. P. Lodge, *Macromolecules*, 2022, **55**, 4766–4775.
58 S. Xie, B. Zhang, F. S. Bates and T. P. Lodge, *Macromolecules*, 2021, **54**, 6990–7002.
59 S. Xie, A. P. Lindsay, F. S. Bates and T. P. Lodge, *ACS Nano*, 2020, **14**, 13754–13764.